Iranian Journal of Oil & Gas Science and Technology, Vol. 9 (2020), No. 2, pp. 119–135
http://ijogst.put.ac.ir

Effect of Graphene Oxide Decorated With Synthesized Nano-CeO_2 on Barrier Properties of Epoxy Anticorrosion Coatings

Zeinab Nassaj[1], Fatemeh Ravari[2*], and Iman Danaee[3]

[1] Ph.D. Student, Department of Chemistry, Payame Noor University, Tehran, P.O. Box 19395-4697, Iran
[2] Associate Professor, Department of Chemistry, Payame Noor University, Tehran, P.O. Box 19395-4697, Iran
[3] Associate Professor, Abadan Faculty of petroleum Engineering, petroleum university of Technology, Abadan, Iran

Received: May 30, 2019; *revised*: July 26, 2019; *accepted*: September 16, 2019

Abstract

In this paper, graphene oxide decorated with cerium oxide (CeO_2) nanoparticles was prepared and used as anticorrosive pigments in epoxy nanocomposite coatings. The synthesized nanoparticle was characterized by FTIR, XRD, SEM, and EDX analyses. Graphene oxide decorated with CeO_2 nanoparticles was dispersed in epoxy resin by sonication. The optimum nanoparticle content of the epoxy resin was studied by differential scanning calorimetry. The anticorrosive properties of these coatings were investigated using electrochemical impedance spectroscopy method and polarization in corrosive solution. Impedance parameters showed a decrease in the coating resistance over immersion time. The results indicated that the epoxy coatings containing nanoparticles could significantly increase the corrosion resistance of composite coatings compared to those of pure epoxy, and the highest value was obtained for 1% nanocomposite coatings after 270 days of immersion. Pull-off adhesion test showed that the highest value of adhesion was related to the coating containing 1% nanoparticles.

Keywords: Adhesion, Coatings, Corrosion, Graphene Oxide Decorated with CeO_2 Nanoparticles, Impedance

1. Introduction

Steel has been widely employed as a construction material for pipe work in the oil and gas production such as downhole tubular, flow lines, and transmission pipelines. Steel pipelines play an important role in transporting gases and liquids throughout the world (Ubaid et al., 2019).

Different effective methods such as using inhibitors, applying anodic/cathodic protection, coatings with a proper design have been used to control corrosion of coatings (Ye et al., 2019; Ebrahiminiya et al., 2018; Mahulikar et al., 2011). Coatings are widely employed for corrosion protection in oil and gas industries. The strength of coating/metal system and its lifetime depends on contact time of the system with the corrosive medium, and the adhesion, barrier, and inhibiting properties of the coatings. Aging and diffusion of corrosive agents into the interface between the coating and substrate can lead to

* Corresponding author:
Email: fatemeravari@yahoo.com

blistering, a reduction in the stability of the adhesion bond, an increase in the speed of cathodic reaction, and the degradation of the coating and substrate.

In order to enhance the barrier properties of polymeric coatings, various kinds of additives such as extenders and inorganic pigments have been used (Wang et al., 2019; Huang et al., 2011; Omrani et al., 2013; Sun et al., 2014). In comparison to conventional pigments, the addition of nanoparticles into polymeric coatings offers a more economical method and more durable protection against corrosion (Bakhshandeh et al.; 2014, Ghanbari et al., 2015). With the addition of small amounts of a nanofiller into different polymer matrices, a substantial increase in various physical and chemical properties, including thermal stability, mechanical properties, and barrier and solvent resistance of the as-prepared nanocomposites is noticed (Ravari et al., 2012). Various nanoparticles, including TiO_2, ZnO, ZrO_2, CeO_2, $CaCO_3$, Fe_2O_3, and SiO_2 have, therefore, been employed as reinforcements in order to improve coatings' performance in corrosive environments. It has been shown that the addition of cerium oxide (CeO_2) nanoparticles leads to a decrease in the abrasion resistance of the sol-gel coatings (Schem et al., 2008). The corrosion protection and electrochemical mechanism of a solvent-borne alkyd composite coating containing 1 wt.% polyaniline and 1 wt.% CeO_2 nanoparticles were investigated when it was applied to carbon steel. Moreover, it has been reported that $tCeO_2$ nanoparticles strengthen the barrier-type protection of coatings by blocking water penetration and impeding electrolyte transport in NaCl solution (Li et al., 2019).

Recently, a considerable body of research has been reported on the fabrication of graphene/polymer composites with improved mechanical properties, electrorheological properties, barrier properties, and specific surface area. Unfortunately, it is difficult to disperse and functionalize graphene due to its intrinsically high chemical stability and hydrophobic surface state. Graphene oxide (GO) is one of the most important graphene derivatives which contains an inhomogeneous binding of oxygen functional groups such as hydroxyl, carboxyl, and epoxide groups at the basal planes or edges of the sheets of graphene. The corrosion resistance of pure epoxy coating, GO/epoxy, and GO-Graphene /epoxy were compared by electrochemical impedance spectroscopy (EIS) and salt spray test. The results revealed that the GO-Gr/epoxy exhibited the highest corrosion resistance owing to the synergistic effect of GO and Gr (Zhong et al., 2019). In another work, the incorporation of 0.4 wt.% of (3-aminopropyl) triethoxysilane (APTS)–GO into the polyvinylidene fluoride (PVDF) matrix led to a significant decrease in wettability with water. The contact angle was increased to 102º as compared to 62º for 0.4 wt.% GO and 80º for the neat PVDF (Chiong et al., 2017). Zhang et al. (2019) investigated the anticorrosion property of the waterborne acrylic acid coating by the incorporation of graphene oxide functionalized by polyhedral oligomeric silsesquioxane and indicated that anticorrosion behavior significantly improved, and the corrosion rate declined by 32% to 0.49 mm/a. The functionalization of GO can enhance the interfacial interaction between the GO nanosheets and a matrix, thereby achieving better dispersion. To preclude GO sheets from agglomeration in polymer and achieve an effective interaction between GO and polymer matrix, the nanoparticle-decorated sheets are employed (Chang et al., 2012; Di et al., 2016; Yu et al., 2015; Seza et al., 2015).

The aim of this work is to investigate the effect of graphene oxide decorated with CeO_2 nanoparticles on the corrosion protection of epoxy nanocomposite coatings. Epoxies are widely used as the resin of different protective coatings since they show excellent adhesion, mechanical properties, and chemical resistance in different media. Firstly, graphene oxide decorated with CeO_2 nanoparticles was synthesized, and the prepared nanocomposite coatings were applied on steel plates. The optimum concentration of nanoparticles was investigated by dynamic differential scanning calorimetry (DSC) technique. The inhibition action of the synthesized nanoparticles was also studied by electrochemical

impedance spectroscopy and polarization curves. Finally, to investigate the adhesion of nanocomposite coatings to steel, pull-off tests were employed.

2. Experimental methods

2.1. Materials

Cold rolled carbon steel panels were used as the metallic substrates. The steel substrates were abraded with different types of sandpaper of 120, 220, 320, 400, and 800 grades followed by toluene and acetone degreasing to remove any trace of surface oxides. A liquid epoxy resin and epoxy hardener, graphene oxide powders (purity of 99.5%), N, N-dimethyl formamide (DMF), hydrogen peroxide (H_2O_2), anhydrous ethanol (analytical reagent grade), silane coupling agents (3-aminopropyl) triethoxysilane (APTS) and nano-CeO_2 (with a particle size of about 10–30 nm) were purchased. All materials were commercially available and used without further purification.

2.2. Preparation of GO-CeO_2 composite coating

Firstly, 0.4 g of nano-CeO_2 and 8 g of APTS were dissolved in 200 g of anhydrous ethanol to form a homogenous suspension via ultra-sonication, and the mixture was stirred using a mechanical stirrer at 78 °C for 4 h. In the meantime, 16 g of deionized water was slowly added into the above solution, followed by filtration; the solution was then flushed with anhydrous ethanol and deionized water for six times and dried in a vacuum oven at 60 °C for 24 h to obtain f-CeO_2.

Briefly, the f-CeO_2 (0.2 g) was dispersed in 500 ml DMF to form a homogeneous suspension via ultrasonication for 15 min, and then GO (0.8 g) was added into the suspension via ultrasonication over a period of 30 min. Subsequently, the solution was stirred for 5 h at 105 °C. Finally, the product was obtained by filtrating, washed with anhydrous ethanol seven times, and dried 24 h at 60 °C in a vacuum oven. The final weight ratio of CeO_2 to graphene oxide is 0.5.

To prepare the nanoparticle/epoxy nanocomposites, a pre-determined amount of the nanoparticle was added to the epoxy resin and mixed for 45 min by using a high shear impeller in a variable speed (900–1000 rpm) mixer. The resultant mixture was subjected to sonication for 45 min. Subsequently, a stoichiometric amount of the hardener was then added to the mixture with the mass ratio of the hardener to the epoxy resin of 50:100 and mixed. In order to reduce air bubbles, the mixture was kept in a vacuum chamber for 10 minutes. The coatings were applied on the steel sheets by means of an adjustable film applicator. The thickness of dry coatings was measured with Elcometer FN 4653 digital coating thickness meter (Elcometer Co. Ltd.). A dry film thickness of 20 ± 2 µm was obtained for all the panels. To ensure the film curing, precuring of the nanocomposite was conducted in the laboratory atmosphere for a week before beginning the tests. At the end of the preparation, five formulations with 0, 0.5, 1, 3, and 5 wt.% nanocomposite coating were prepared.

2.3. Corrosion tests

Electrochemical impedance spectroscopy is known as a powerful and nondestructive useful technique for studying, measuring, and estimating coating resistance. The EIS and polarization measurements were performed at room temperature using an Autolab PGSTAT 302N Potentiosat/Galvanostat coupled with a FRA2 frequency response analyzer at open circuit potential. The measuring cell for corrosion consisted of the coated sample panel as a working electrode immersed in 3.5% NaCl solution, a platinum as the counter electrode, and a saturated calomel electrode (SCE) as a reference electrode. The measuring frequency was ranged from 100 kHz to 10 mHz with an AC amplitude of 10 mV. The impedance diagrams were obtained at different exposure times of up to 270 days.

2.4. Pull-off adhesion test

The pull-off adhesion tests were performed before and after immersion in the corrosive solution to measure the adhesion strength of the epoxy coatings with various nanoparticle content values. These tests were conducted using an Elcometer 106 Adhesion Tester with a maximum applied load of 20 MPa in accordance with ASTM D4541 type III. The dolly fixture with an area of 0.5 cm^2 was glued to the surface of the coated specimen using an appropriate adhesive (Cyanoacrylate MC1500). In the case of adhesion measurement after exposure, the samples were removed from the solution after 35 days of immersion, rinsed completely with deionized water, and allowed to dry for 48 h at ambient temperature. For each type of coatings, measurements were conducted three times, and the average was calculated.

3. Results and discussions

3.1. Characterization of nanoparticle

The nano-CeO_2 modified with ATPS was characterized using FTIR. Figure 1 shows the FTIR spectra of ATPS and treated and untreated CeO_2. ATPS illustrates different characteristic peaks containing a stretching bond of C–O at 1150 cm^{-1}, a stretching bond of C–N at 1300 cm^{-1}, a stretching bond of C–H at 3000 cm^{-1}, a stretching bond of adsorbed CO_2 at 2400 cm^{-1}, and the bending of C–H at 1400 cm^{-1} (Figure 1a). Moreover, the main characteristic peaks which are observed at 450 and 800 cm^{-1} are due to Si–O and Si–O–H bonds respectively. A broad peak in the FTIR spectra of ATPS at 1100 cm^{-1} is related to the Si–O–C stretching or asymmetric Si–O–Si stretching vibration (polymerized form) (Kurth et al., 1995). In addition, the broad bands at 3400 and 1600 cm^{-1} can be ascribed to the N–H stretching vibration and NH_2 bending mode of free NH_2 group respectively (Salili et al., 2015). The important peaks of cerium oxide (Chelliah et al., 2012) are the stretching bond of Ce–O at 550 cm^{-1} and the stretching vibration of –OH groups at 3500 cm^{-1} (Figure 1b).

a)

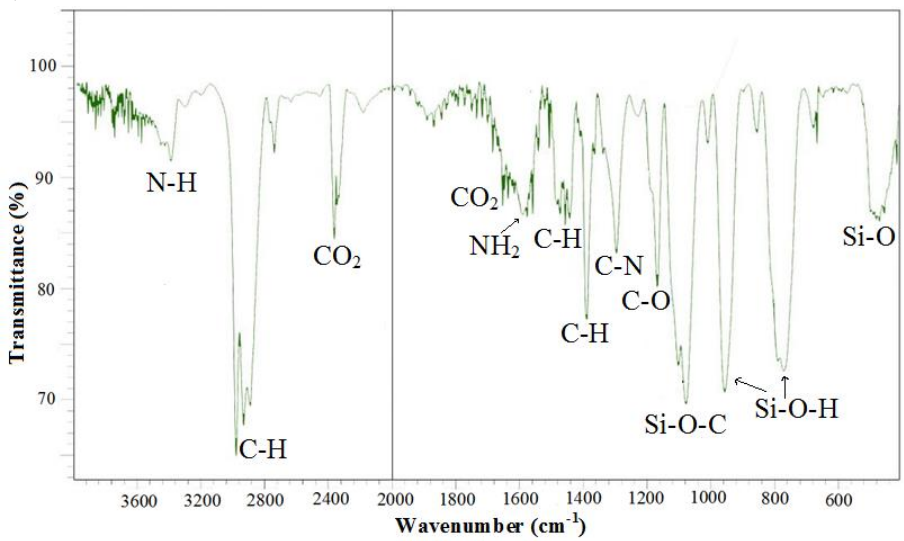

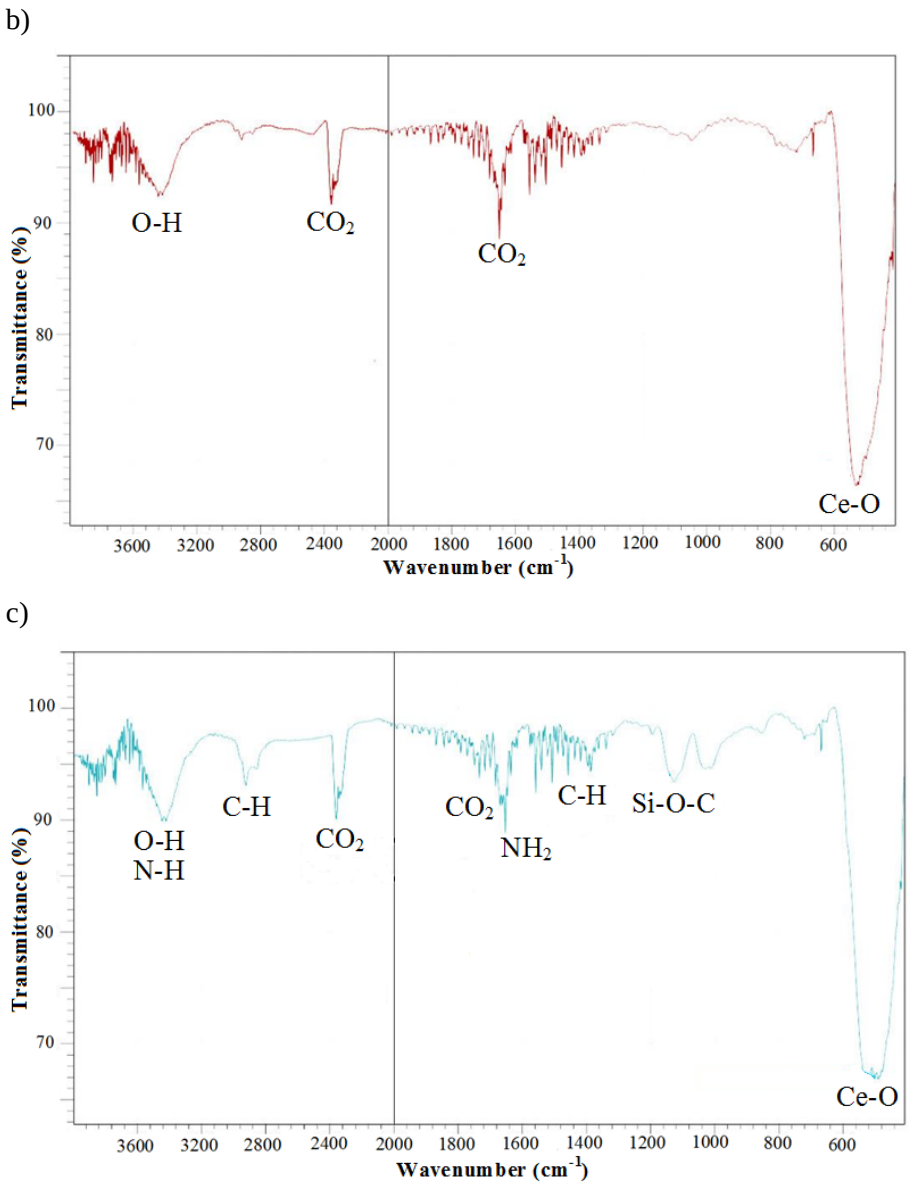

Figure 1

FTIR spectra of (a) ATPS, (b) nano-CeO_2, and (c) f-CeO_2.

Most of the important FTIR peaks of ATPS are repeated for the modified CeO_2 (Figure 1c), which indicates effective bonding between these chemicals. The bands at around 3000 cm^{-1} observed in the FTIR spectrum of the treated particle can be associated with the alkyl groups [$–(CH_2)_n–$] of the ATPS on the surface. Moreover, the observation of a band around 1100 cm^{-1} can be attributed to the Si–O–C stretching or the asymmetric Si–O–Si stretching vibration of ATPS on the surface of nanoparticles. This indicates the successful coating of APTS on the nano-CeO_2 surface through chemical bonding.

On a graphene oxide sheet, the amounts of hydroxyl are much more than epoxide and carboxyl groups. In addition, epoxide and carboxyl groups are heterogeneously distributed on the surface of GO. Epoxide and carboxyl groups have a higher reaction activity than hydroxyl and provide a handle for further surface chemical functionalization via well-developed carbon chemistry. For the uniform and efficient connection of nanoparticles with GO sheets, it is indispensable to increase the amount of epoxide groups, and this goal can be achieved with the help of 3-aminopropyltrimethoxysilane. Therefore, the CeO_2–GO nanocomposites were synthesized by using 3-aminopropyltriethoxysilane. In this process,

the amine group of APTS is conjugated with the handle, i.e. oxygen functional groups, on the graphene sheets.

Figure 2a indicates the graphene sheet modified with CeO_2 nanoparticles. As can be seen, nanoparticles are connected to the graphene surface. Figure 2b shows the energy dispersive X-ray (EDX) analysis of graphene sheets modified with CeO_2 nanoparticles. According to the EDX diagram, cerium oxide is effectively detected on carbon substrates. Figure 2c illustrates the TEM image of CeO_2 nanoparticles. It is clear that the particle size is about 30–40 nm.

a)

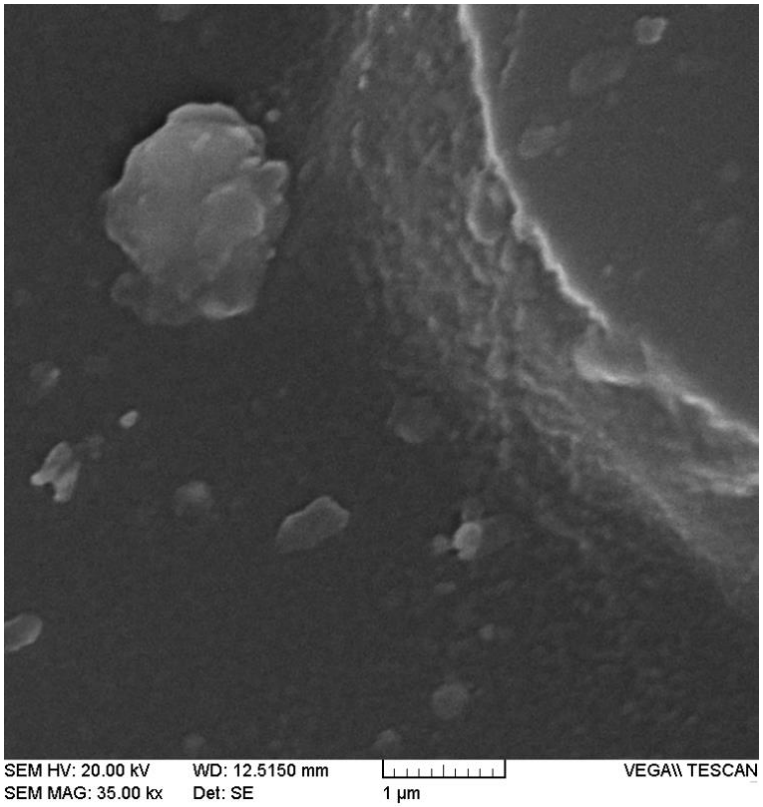

b)

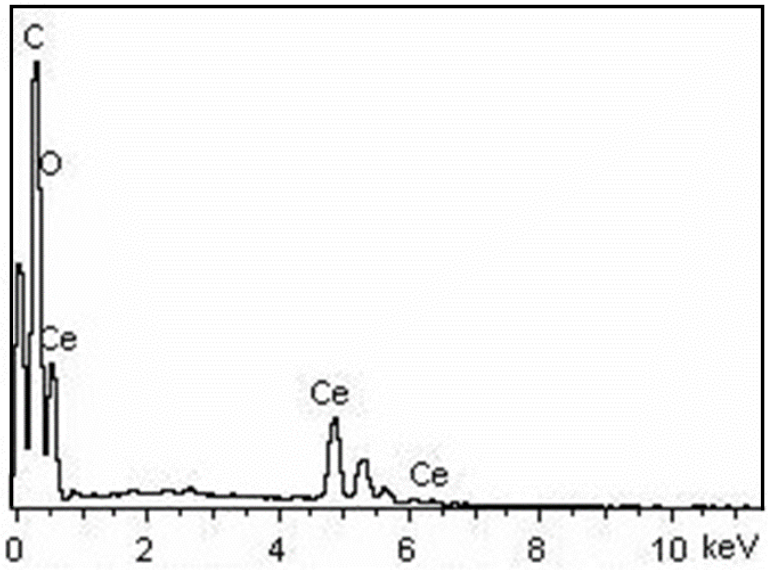

c)

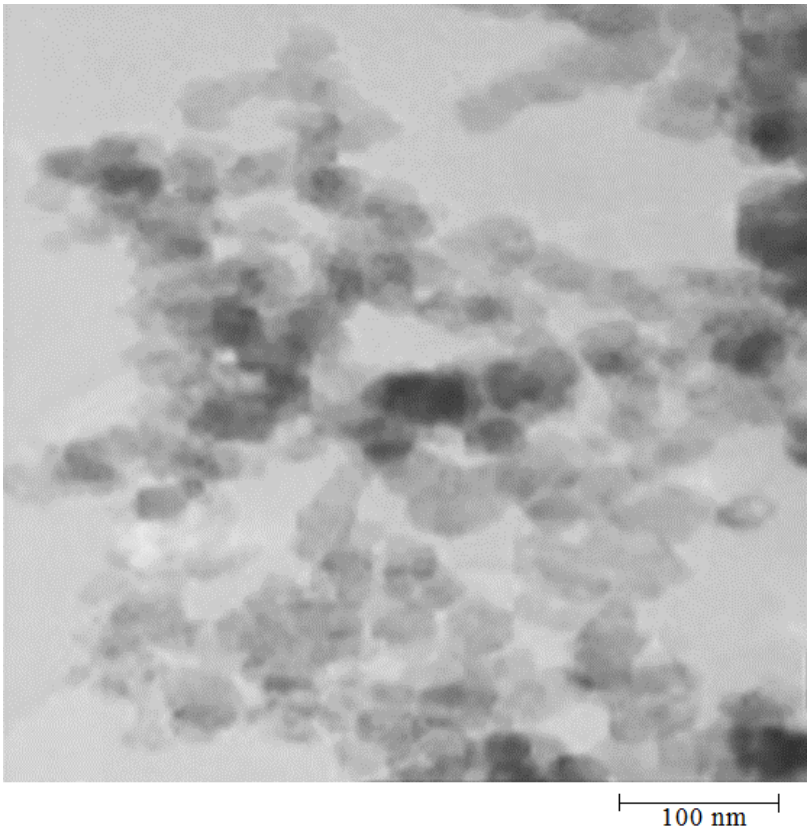

Figure 2

a) SEM micrographs of CeO_2–GO surface, b) the EDX analysis of CeO_2–GO, and c) the TEM image of CeO_2 nanoparticles.

Figure 3 shows the XRD patterns of graphene oxide (GO), cerium oxide (CeO_2), and hybrid **(**CeO_2–GO). A Philips diffractometer with Cu Kα radiation (λ = 1.54060 Å) was used. The XRD pattern of graphene oxide (Figure 3a) shows a sharp diffraction peak (001) at 2θ = 11.58° corresponding to an interlayer *d*-spacing of 7.7 Å and the (100) diffraction peak at 2θ = 42.0° according to a *d*-spacing of 2.13 Å, which confirms the characteristic peaks of GO (Ain et al., 2019). In the XRD pattern of CeO_2 (Figure 3b), the characteristic peaks matched well the literature value JCPDS card No. 34-0394 for CeO_2. The diffraction angles at 2θ = 28.56, 33.08, 47.47, 56.36, 59.08, 69.41, 76.69, 79.07, and 88.39° can be respectively assigned to (111), (200), (220), (311), (222), (400), (331), (420), and (422) of the crystal planes of cerium oxide (Tamizhdurai et al., 2017), which correspond to the face-centered cubic phase of CeO_2 crystal with *d*-spacing vales 3.12, 2.71, 1.91, 1.63, 1.56, 1.35, 1.24, 1.21, and 1.11 Å respectively.

The XRD pattern of CeO_2–GO (Figure 3c) is in agreement with the XRD patterns of CeO_2 and graphene oxide, including all the characteristic peaks. These results confirm the successful synthesis of hybrid CeO_2–GO. The average crystallite size of CeO_2–GO is calculated by using Debye Scherrer formula as 38.93 nm.

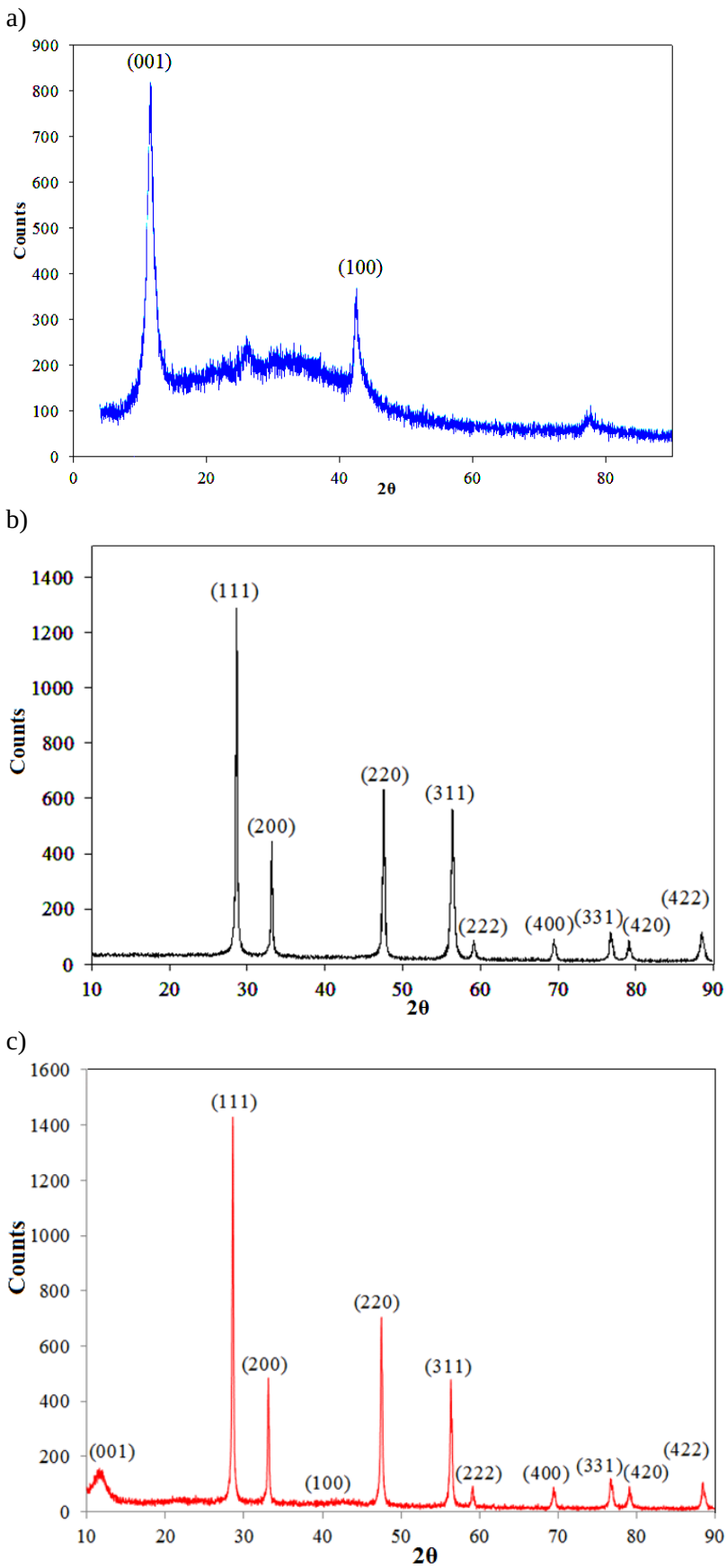

Figure 3

The XRD patterns of a) graphene oxide (GO), b) cerium oxide, and c) hybrid (CeO_2–GO).

The optimal content of the composite samples is studied using differential scanning calorimetry analysis. Figure 4 shows the heat flow of the various samples versus temperature. The effects of the nanohybrid CeO_2–GO on the curing reaction rate can be clearly observed. As can be seen, the heat flow of nanocomposites starts to increase at about 45 °C and reaches its maximum at about 94 °C. Moreover, the heat flow improves in the presence of nanohybrids up to 1 wt.%, but it drops at higher amounts of nanohybrid CeO_2–GO. It can be seen that 1 wt.% CeO_2–GO epoxy nanocomposite indicates a maximum heat reaction and thus a faster reaction rate, which leads to a decrease in the necessary time to reach complete conversion compared to the other samples. The high amount of heat reaction shows higher interaction between the nanoparticle and the epoxy resin, so the sample is highly stable. Enthalpy value decreases in the presence of higher weight ratio of nanohybrid CeO_2–GO due to low dispersion and/or cluster or agglomerate formation of nanoparticles in the epoxy matrix. Table 1 illustrates the heat reaction of nanocomposite samples, where T_i represents the onset temperature, T_m is the peak temperature, T_f is the final cure temperature, and ΔH is the heat of curing.

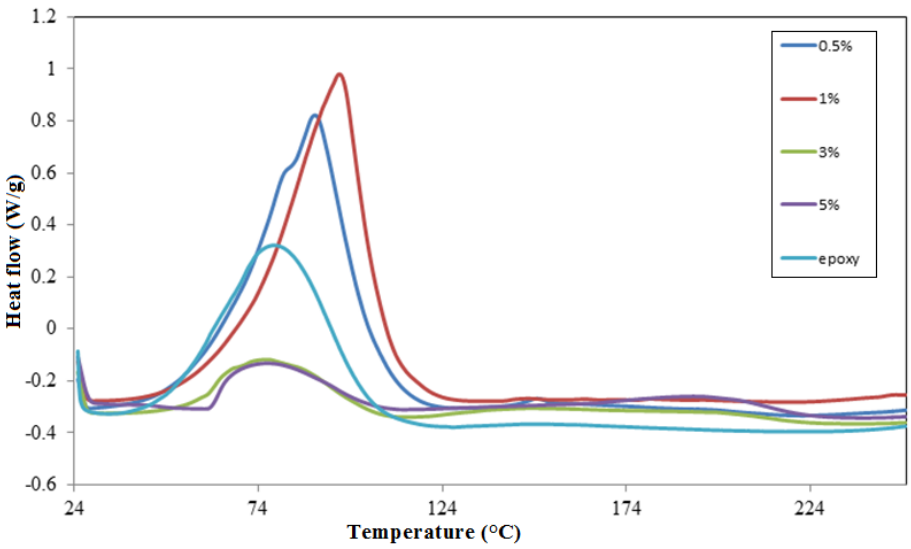

Figure 4

DSC curves of the epoxy nanocomposites with different amounts of the nanoparticle.

Table 1

Parameters obtained from DSC nonisothermal experiment.

Sample	Heating rate (β) (°C/min)	Onset temperatures (T_i) (°C)	Peak temperatures (T_m) (°C)	Final cure temperatures (T_f) (°C)	ΔH_{total} (J/g)
0.5%	10	61.90	89.38	106.99	201.20
1%	10	67.00	96.10	109.16	208.61
3%	10	56.73	76.30	104.72	43.16
5%	10	61.27	76.63	104.48	30.49
Epoxy	10	52.13	78.58	104.98	138.87

3.2. Electrochemical impedance spectroscopy measurements

The Bode plots of the steel samples in 3.5 wt.% NaCl solutions with 1% nanopigments at different immersion times are presented in Figure 5. It is obvious that all the Bode plots are in the form of one-time constants, which is indicative of the coating resistance (R_c) against electrolyte diffusion.

With increasing immersion time up to 270 days, the coating impedance values decrease depending on the diffusion of water and corrosive ions into the coating. The electrical equivalent circuits used for numerical fitting of the impedance plots at different exposure times are shown in Figure 6 where R_s, R_c, and Q_c represent solution resistance between the reference electrode and working electrode, coating resistance, and the constant phase element of the coating capacitance respectively. Table 2 tabulates the various electrochemical impedance parameters for different exposure times. A constant phase element (CPE) defined by the following equation is often used instead of a capacitance to account for the nonideal capacitive response from the interface:

$$Z_{cpe} = \frac{1}{Y_0 (j\omega)^n}$$

where Z represents the impedance of the CPE, ω is angular frequency (ω=2πf), *n* stands for CPE power, and Y_0 is CPE constant which is a combination of properties related to both the surface and the electroactive species. The exponential factor *n* is often related to the degree of heterogeneity of the interface and/or surface film, that is, the larger the deviation from one, the more heterogeneous the surface layer (Zamanizadeh et al., 2014). According to Table 2, R_c of the steel panels coated with the epoxy/nanoparticle nanocomposite coatings decreases as the immersion time extends. This indicates that the protective properties of the coating gradually decrease with increasing immersion times.

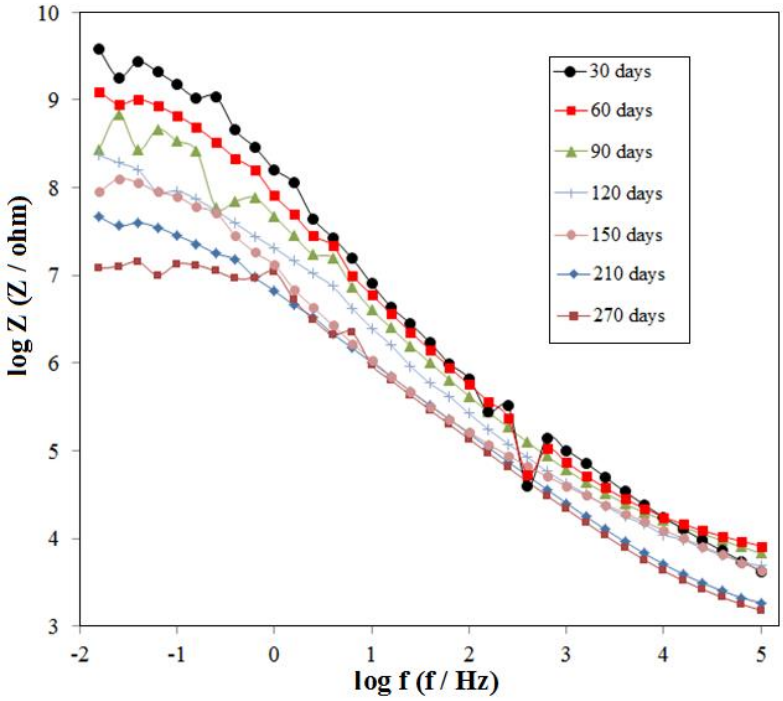

Figure 5

Bode plots of the 1% nanocomposite coating at different immersion times in the 3.5 wt.% NaCl solutions.

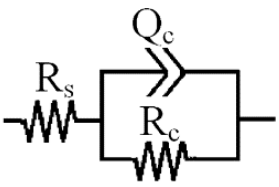

Figure 6

Equivalent circuits used for fitting the impedance plots obtained at different immersion times.

Table 2

Electrochemical parameters extracted from the EIS data for the 1% nanocomposite coating at different immersion times.

	R_c	Q_c	n
30 days	5.42×10^{9}	9×10^{-8}	0.81
60 days	1.66×10^{9}	8×10^{-8}	0.78
90 days	8.78×10^{8}	6×10^{-8}	0.75
120 days	9.86×10^{7}	4×10^{-8}	0.76
150 days	7.64×10^{7}	5×10^{-8}	0.73
210 days	6.63×10^{7}	2×10^{-8}	0.7
270 days	2.19×10^{7}	9×10^{-7}	0.71

The capacitance values of all the samples increase by increasing immersion. This can be attributed to water diffusion which has a higher dielectric constant compared to polymeric coatings (Zamanizadeh et al., 2014). The variation of parameter *n* of the constant phase element with time (Table 2) shows that it decreases with an increase in immersion time. This can be attributed to increase in surface heterogeneity and coating degradation as a result of the diffusion of the corrosive electrolyte into the coating matrix.

Figure 7 delineates the effect of nanoparticles with different weight ratios on the barrier properties of the epoxy coatings after 270 days of immersion in a corrosive solution. By comparing the Bode plots, it can be seen that over a long period of immersion time (270 days), higher coating resistance is obtained in the presence of graphene oxide decorated with CeO_2 nanoparticles (Table 3). This means that nanoparticles could significantly enhance the barrier properties of the epoxy coating by forcing the corrosive agents to travel a longer tortuous path to reach the substrate. In addition, nanoparticles fill the holes of the coating and lead to the enhancement of coating resistance. Cerium oxide nanoparticles prevent the agglomeration of graphene oxide, so the dispersion ability of the modified nanohybrid CeO_2–GO is improved. In the absence of cerium oxide, graphene oxide has a high surface with low interaction with the polymer matrix, which leads to a reduction in the coating dispersion.

Table 3

Electrochemical parameters extracted from the EIS data at different amounts of nano CeO_2–GO after 270 days of immersion.

	R_c (or combination of R_c and R_{ct})	Q_c (or combination of Q_c and Q_{dl})	n
Neat epoxy	3.82×10^{4}	4×10^{-5}	0.55
0.5%	7.53×10^{6}	5×10^{-7}	0.68
1%	2.19×10^{7}	9×10^{-7}	0.71
3%	9.21×10^{5}	6×10^{-6}	0.65
5%	7.44×10^{5}	8×10^{-6}	0.66

By increasing the concentration of nanoparticles up to 1 wt.%, the impedance of the coating increases. In addition, it can be seen that the capacitance values of the coating containing 1 wt.% nanoparticle are less than the other samples. However, due to the barrier properties of the nanoparticles, water diffusion rate is less than the neat epoxy. In the presence of higher amounts of nanoparticles, the porosity of the coating increases, so corrosion resistance drops and the coating capacitance rises.

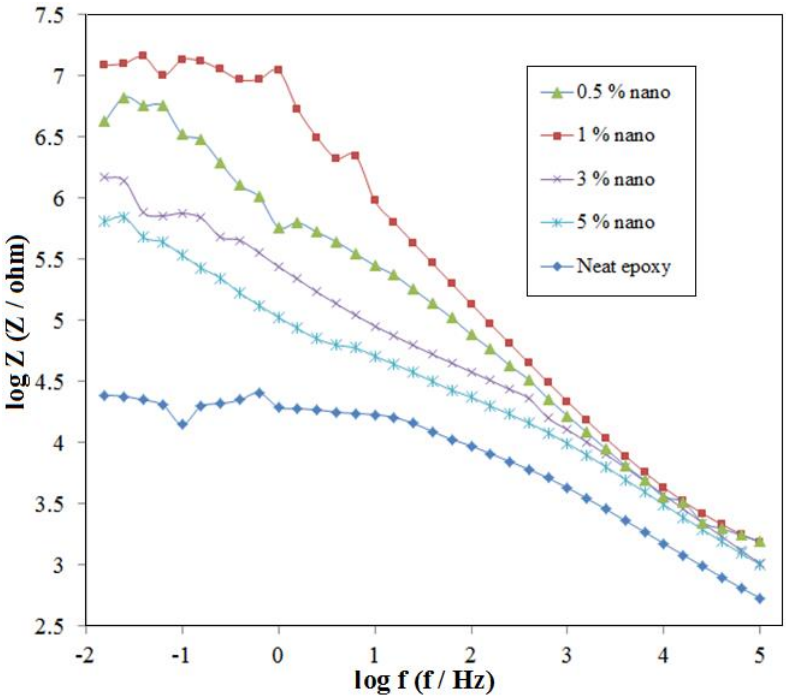

Figure 7

Bode plots of the epoxy coatings at different amounts of nanoparticles after 270 days of immersion in the 3.5 wt.% NaCl solutions.

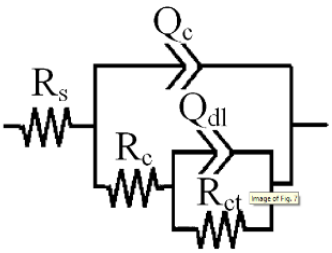

Figure 8

Equivalent circuits used for fitting the impedance plots obtained at very long immersion times.

At very long immersion time, the coating resistance decreases significantly especially for the neat epoxy and 3 and 5% nanocomposites due to the penetration of water and corrosive ions, which starts corrosion reactions under the coating. In this situation, charge transfer resistance and double layer capacitance are necessary in an equivalent circuit for considering corrosion reactions. Figure 8 shows the equivalent circuit at very long immersion times. In this equivalent circuit, R_{ct} and Q_{dl} indicate the charge transfer resistance and double layer capacitance. Therefore, the calculated resistance in Table 3 can be the combination of charge transfer resistance and coating resistance. Due to the strong overlapping of these time constants, separate calculation of the coating and charge transfer resistance is not exact, so it is presented in a combination form.

3.3. Tafel polarization curves

Figure 9 shows Tafel polarization curves of the neat epoxy coating, the epoxy coatings containing 1 wt.% graphene oxide, 1% cerium oxide, and 1% graphene oxide modified with cerium oxide in 3.5% NaCl solution. The data are recorded at a scanning rate of 1 mV s^{-1}. Tafel calculations are listed in Table 4, where E_{corr} and I_{corr} are the corrosion potential and corrosion current density respectively. The corrosion current density falls, but the corrosion potential rises in the presence of nanoparticles. The

enhancement of corrosion protection is related to an increase in the tortuosity of the diffusion pathways of corroding agents due to the presence of the dispersed nanoparticles. The epoxy nanocomposite with graphene oxide indicates suitable protection ability related to the flakes and layers properties of GO, which leads to a strong barrier effect in the epoxy coatings. The quality of GO dispersion in the polymer coating is the main concept for achieving desirable barrier properties and corrosion protection in nanocomposite coatings (Pourhashem et al., 2017; Jiang et al., 2019). CeO_2 nanoparticle has a spherical shape, so its barrier effect in epoxy is lower than graphene oxide. Cerium oxide on graphene oxide surface improves the dispersion of GO and helps separate flakes and layers of graphene, so it enhances the barrier effect of the nanohybrid CeO_2–GO. In addition, the interaction between GO and polymer matrix can be increased in the presence of CeO_2. As seen from Table 4, the nanocomposite containing graphene oxide modified with cerium oxide shows the highest inhibition effect among the coatings.

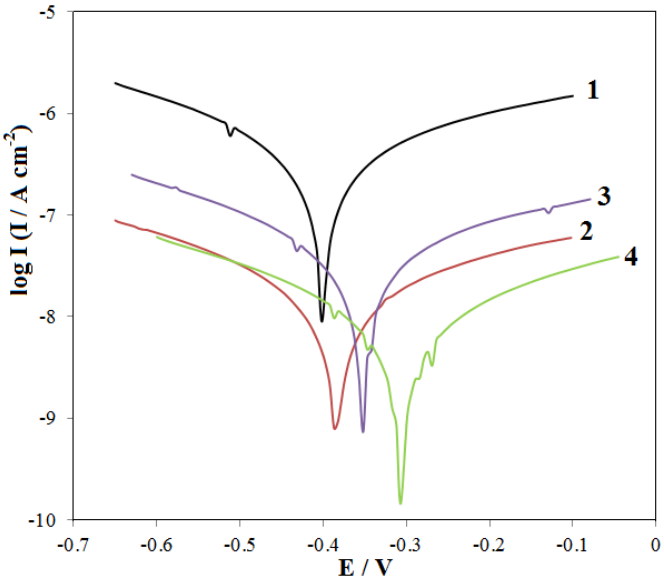

Figure 9

Tafel polarization curves of 1) the neat epoxy and the epoxy coatings containing 1 wt.% of 2) graphene oxide, 3) cerium oxide, and 4) graphene oxide modified with cerium oxide in the 3.5 wt.% NaCl solutions.

Table 4

Polarization parameters extracted from the Tafel data for different coatings.

	I_{corr} (A cm^{-2})	E_{corr} (V)
Neat epoxy	1.41×10^{-7}	–0.402
Epoxy containing 1% graphene oxide	5.82×10^{-9}	–0.387
Epoxy containing 1% cerium oxide	1.38×10^{-8}	–0.352
Epoxy containing 1% graphene oxide modified with cerium oxide	2.45×10^{-9}	–0.307

3.4. Adhesion measurement

Adhesion tests were performed on the epoxy resin in the presence of different loadings of nanoparticles. The adhesion tests prior to exposure and after 35 days of exposure to an corrosive environment are summarized in Table 5. The exact determination of adhesion strength prior to exposure to 5 wt.% NaCl is not possible since the coatings are always cohesive. After 35 days of exposure to the corrosive environment, the wet adhesion of the coating to the substrate decreases due to the penetration of the corrosive agents and the initiation of steel corrosion under the coating. It is observed that a higher wet

adhesion of the coating to the substrate is obtained in the presence of nanoparticles, so the penetration of corrosive agents decreases. The sample loaded with 1% nanoparticle shows the best wet adhesion of the coating to the substrate.

Table 5

Dry and wet adhesion and the percentage of adhesion reduction after 35 days of exposure to 5% NaCl solution.

Nanoparticle content (wt.%)	Dry adhesion (N mm^{-2})	Wet adhesion (N mm^{-2})	Adhesion reduction (%)
0	3.85	0.99	74.28
0.5	3.88	1.82	53.09
1	3.65	2.16	40.82
3	3.44	1.66	51.74
5	3.77	1.51	59.94

4. Conclusions

In this study, graphene oxide decorated with CeO_2 nanoparticles was used as a pigment in the epoxy resin. The following conclusions can be drawn based on the results obtained:

- Graphene sheets were effectively modified with cerium oxide nanoparticles, and epoxy nanocomposites were prepared with modified graphene sheets.
- DSC analysis indicated that the maximum heat of reaction for the epoxy nanocomposite was related to the sample containing 1 wt.% nanoparticle.
- The addition of the nanoparticle significantly improved the anticorrosive properties of the epoxy coating. The equivalent circuit elements showed that the coating containing 1 wt.% nanoparticle had a higher value of coating resistance and lower capacitance in comparison with the other samples.
- According to the polarization curves, the epoxy nanocomposite made of nanohybrid CeO_2–GO shows a higher inhibition effect compared with the epoxy nanocomposite containing graphene oxide.
- According to the results of the wet pull-off test, the decrease in the wet adhesion strength of the neat epoxy coating was more severe compared to the nanocomposites. Thus, nanoparticle can reduce the adhesion loss of the coating due to an increase in the barrier properties.

Nomenclature

E_{corr}	Corrosion potential
I_{corr}	Corrosion current density
Q_c	Constant phase element of coating capacitance
R_c	Coating resistance
R_s	Solution resistance
T_f	Final cure temperature
T_i	Onset temperature
T_m	Peak temperature
ΔH	Heat of curing
ω	Angular frequency

References

Ain, Q.T., Haq, S.H., Alshammari, A., Al-Mutlaq, M.A., and Anjum, M.N., The Systemic Effect of PEG-nGO-Induced Oxidative Stress in Vivo in a Rodent Model, Beilstein Journal of Nanotechnology, Vol. 10, p. 901–911, 2019.

Bakhshandeh, E., Jannesari, A., Ranjbar, Z., Sobhani, S., and Saeb, M. R., Anticorrosion Hybrid Coatings Based on Epoxy-silica Nanocomposites: Toward Relationship between the Morphology and EIS Data, Progress in Organic Coatings, Vol. 77, p. 1169–1183, 2014.

Chang, C. H., Huang, T. C., Peng, C. W., Yeh, T. C., Lu, H. I., Hung, W. I., and Yeh, J. M., Novel Anticorrosion Coatings Prepared from Polyaniline/Graphene Composites, Carbon, Vol. 50, No. 14, p. 5044–5051, 2012.

Chelliah, M., Rayappan, J.B.R., and Krishnan, U.M., Synthesis and Characterization of Cerium Oxide Nanoparticles by Hydroxide Mediated Approach, Journal of Applied Sciences, Vol. 12, p. 1734–1737, 2012.

Chiong, S.J., Goh, P.S., and Ismail, A.F., Novel Hydrophobic PVDF/APTES–GO Nanocomposite for Natural Gas Pipelines Coating, Natural Gas Science and Engineering, Vol. 42, p. 190–202, 2017.

Di, H., Yu, Z., Ma, Y., Li, F., Lv, L., Pan, Y., and He, Y.., Graphene Oxide Decorated with Fe_3O_4 Nanoparticles with Advanced Anticorrosive Properties of Epoxy Coatings, Journal of the Taiwan Institute of Chemical Engineers, Vol. 64, p. 244–251, 2016.

Ebrahiminiya, A., Khorram, M., Hassanajili, S., and Javidi, M., Modeling and Optimization of the Parameters Affecting the In-situ Microencapsulation Process for Producing Epoxy-based Self-healing Anticorrosion Coatings, Particuology, Vol. 36, p. 59–69, 2018.

Ghanbari, A. and Attar, M. M., A Study on the Anticorrosion Performance of Epoxy Nanocomposite Coatings Containing Epoxy-silane Treated Nanosilica on Mild Steel Substrate, Journal of Industrial and Engineering Chemistry, Vol. 23, p. 145–153, 2015.

Huang, T. C., Su, Y. A., Yeh, T. C., Huang, H. Y., Wu, C. P., Huang, K. Y., and Wei, Y., Advanced Anticorrosive Coatings Prepared from Electroactive Epoxy-SiO_2 Hybrid Nanocomposite Materials, Electrochimic Acta, Vol. 56, No. 17, p. 6142–6149, 2011.

Jiang, F., Zhao, W., Wu, Y., Dong, J., Zhou, K., Lu, G., and Pu, J., Anticorrosion Behaviors of Epoxy Composite Coatings Enhanced via Graphene Oxide with Different Aspect Ratios, Progress in Organic Coatings, Vol. 127, p. 70–79, 2019.

Kurth, D.G. and Bein, T., Thin Films of (3-Aminopropy1) Triethoxysilaneo No Aluminum Oxide and Gold Substrates, Langmuir, Vol. 11, p. 3061–3067, 1995.

Li, J., Ecco, L., Ahniyaz, A., and Pan, J., Probing Electrochemical Mechanism of Polyaniline and CeO_2 Nanoparticles in Alkyd Coating with In-situ Electrochemical-AFM and IRAS, Progress in Organic Coatings, Vol. 132, p. 399–408, 2019.

Mahulikar, P. P., Jadhav, R. S., and Hundiwale, D. G., Performance of Polyaniline/TiO_2 Nanocomposites in Epoxy for Corrosion Resistant Coatings, Iranian Polymer Journal, Vol. 20, No. 5, p. 367–376, 2011.

Omrani, A., Rostami, A., Ravari, F., and Ehsani, M., The Relationship Between Composition and Electrical Properties of Brass Covered by a Nanocomposite Coating of Glycerol Diglycidyl Ether: An EIS and DMTA Study, Progress in Organic Coatings, Vol. 76, No. 2–3, p. 360–366, 2013.

Pourhashem, S., Vaezi, M.R., Rashidi, A., and Bagherzadeh, M.R., Exploring Corrosion Protection Properties of Solvent based Epoxy-graphene Oxide Nanocomposite Coatings on Mild Steel, Corrosion Science, Vol. 115, p. 78–92, 2017.

Ravari, F., Omrani, A., Rostami, A. A., and Ehsani, M., Ageing Effects on Electrical, Morphological, and Mechanical Properties of a Low Viscosity Epoxy Nanocomposite, Polymer Degradation and Stability, Vol. 97, p. 929–935, 2012.

Salili, S.M., Ataie, A., Barati, M.R., and Sadighi, Z., Characterization of Mechano-thermally Synthesized Curie Temperature-adjusted La0.8Sr0.2MnO_3 Nanoparticles Coated with (3-aminopropyl) Triethoxysilane, Materials Characterization, Vol. 106, p. 78–85, 2015.

Schem, M., Schmidt, T., Gerwann, J., Wittmar, M., and Zheludkevich, M. L., CeO_2-filled Sol-gel Coatings for Corrosion Protection of AA2024-T3 Aluminum Alloy, Corrosion Science, Vol. 51, p. 2304–2315, 2008.

Seza, A., Jafarian, H., Hasheminiasari, M., and Aliofkhazraei, M., Effect of Duty Cycle on Corrosion Resistance and Mechanical Properties of Tertiary Al_2O_3/Y_2O_3/Graphene Pulsed Electrodeposited Ni-based Nano-composite, Procedia Materials Science., Vol. 11, p. 576–582, 2015.

Sun, W., Wang, L., Wu, T., Pan, Y., and Liu, G., Synthesis of Low-electrical-conductivity Graphene/Pernigraniline Composites and Their Application in Corrosion Protection, Carbon, Vol. 79, No. 1, p. 605–614, 2014.

Tamizhdurai, P., Sakthinathan, S., Chen, S.M., Shanthi, K., Sivasanker, S., and Sangeetha, P., Environmentally Friendly Synthesis of CeO_2 Nanoparticles for the Catalytic Oxidation of Benzyl Alcohol to Benzaldehyde and Selective Detection of Nitrite, Scientific Reports, Vol. 7, p. 46372, 2017.

Ubaid, F., Radwan, A. B., Naeem, N., Shakoor, R. A., Ahmed, Z., Montemor, M. F., and Soliman, A., Multifunctional Self-healing Polymeric Nanocomposite Coatings for Corrosion Inhibition of Steel, Surface and Coatings Technology, Vol. 372, p. 121–133 2019.

Wang, W., Wang, H., Zhao, J., Wang, X., Xiong, C., Song, L., and Li, W., Self-healing Performance and Corrosion Resistance of Graphene Oxide–mesoporous Silicon Layer–nanosphere Structure Coating under Marine Alternating Hydrostatic Pressure, Chemical Engineering Journal, p. 792–804, 2019.

Ye, Y., Zhang, D., Liu, T., Liu, Z., Pu, J., Liu, W., and Wang, L., Superior Corrosion Resistance and Self-healable Epoxy Coating Pigmented with Silanized Trianiline-intercalated Graphene, Carbon, Vol. 142, p. 164–176, 2019.

Yu, Z., Di, H., Ma, Y., Lv, L., Pan, Y., Zhang, C., and He, Y., Fabrication of Graphene Oxide-alumina Hybrids to Reinforce the Anticorrosion Performance of Composite Epoxy Coatings, Applied Surface Science, Vol. 351, p. 986–996, 2015.

Zamanizadeh, H. R., Shishesaz, M. R., Danaee, I., and Zaarei, D., Investigation of the Corrosion Protection Behavior of Natural Montmorillonite Clay/Bitumen Nanocomposite Coatings, Progress in Organic Coatings, Vol. 78, p. 256–260, 2015.

Zhang, X., Ma, R., Du, A., Liu, Q., and Cao, X., Corrosion Resistance of Organic Coating Based on Polyhedral Oligomeric Silsesquioxane-functionalized Graphene Oxide, Applied Surface Science, Vol. 484, p. 814–824, 2019.

Zhong, F., He, Y., Wang, P., Chen, C., and Chen, J., Self-assembled Graphene Oxide-graphene Hybrids for Enhancing the Corrosion Resistance of Waterborne Epoxy Coating, Applied Surface Science, Vol. 488, p. 801–812, 2019.